

1 **Experiments and simulations on short chain fatty acid production in a colonic**
2 **bacterial community**

3
4 Bea Yu,^a Ilija Dukovski,^{b,c} David Kong,^d Johanna Bobrow,^a Alla Ostrinskaya,^a Daniel Segre^{b,c,e,#},
5 Todd Thorsen ^{a#}
6

7 ^aMIT Lincoln Lab, 244 Wood Street, Lexington, MA 02421, USA

8 ^bBioinformatics Graduate Program, Boston University, Boston, MA 02215, USA ^cBiological
9 Design Center, Boston University, Boston, MA 02215, USA

10 ^dDirector, Community Biotechnology Initiative, MIT Media Lab, Massachusetts Institute of
11 Technology, 77 Mass. Ave., E14/E15, Cambridge, MA 02139 USA

12 ^eDepartment of Biology, Department of Biomedical Engineering and Department of Physics,
13 Boston University, Boston, MA 02215, USA

14

15 Running Head: Study of *F. prausnitzii*-*B. thetaiotaomicron* coculture

16 #Address correspondence to: Daniel Segre, dsegre@bu.edu and Todd Thorsen,

17 thorsen@ll.mit.edu

18 B.Y. and I.D. contributed equally to this work.

DISTRIBUTION STATEMENT A. Approved for public release. Distribution is unlimited.

This material is based upon work supported by the Assistant Secretary of Defense for Research and Engineering under Air Force Contract No. FA8702-15-D-0001. Any opinions, findings, conclusions or recommendations expressed in this material are those of the author(s) and do not necessarily reflect the views of the Assistant Secretary of Defense for Research and Engineering.

19

20

21 **Abstract**

22 Understanding how production of specific metabolites by gut microbes is modulated by
23 interactions with surrounding species and by environmental nutrient availability is an important
24 open challenge in microbiome research. As part of this endeavor, this work explores interactions
25 between *F. prausnitzii*, a major butyrate producer, and *B. thetaiotaomicron*, an acetate producer,
26 under three different *in vitro* media conditions in monoculture and coculture. *In silico* Genome-
27 scale dynamic flux balance analysis (dFBA) models of metabolism in the system using
28 COMETS (Computation of Microbial Ecosystems in Time and Space) are also tested for
29 explanatory, predictive and inferential power. Experimental findings indicate enhancement of
30 butyrate production in coculture relative to *F. prausnitzii* monoculture but defy a simple model
31 of monotonic increases in butyrate production as a function of acetate availability in the medium.
32 Simulations recapitulate biomass production curves for monocultures and accurately predict the
33 growth curve of coculture total biomass, using parameters learned from monocultures,
34 suggesting that the model captures some aspects of how the two bacteria interact. However, a
35 comparison of data and simulations for environmental acetate and butyrate changes suggest that
36 the organisms adopt one of many possible metabolic strategies equivalent in terms of growth
37 efficiency. Furthermore, the model seems not to capture subsequent shifts in metabolic activities
38 observed experimentally under low-nutrient regimes. Some discrepancies can be explained by
39 the multiplicity of possible fermentative states for *F. prausnitzii*. In general, these results
40 provide valuable guidelines for design of future experiments aimed at better determining the
41 mechanisms leading to enhanced butyrate in this ecosystem.

42

43

44 **Importance**

45 Studies associating butyrate levels with human colonic health have inspired research on
46 therapeutic microbiota consortia that would optimize butyrate production if implanted in the
47 human colon. *Faecalibacterium prausnitzii* is commonly observed in human fecal samples and
48 produces butyrate as a product of fermentation. Previous studies indicate that *Bacteroides*
49 *thetaiotaomicron*, also commonly found in human fecal samples, may enhance butyrate
50 production in *F. prausnitzii* when the two species are co-localized. This possibility is
51 investigated here under different environmental conditions using experimental methods paired
52 with computer simulations of the whole metabolism of bacterial cells. Initial findings indicate
53 that interactions between these two species result in enhanced butyrate production. However,
54 results also paint a nuanced picture, suggesting the existence of a multiplicity of equivalently
55 efficient metabolic strategies and complex interactions between acetate and butyrate production
56 in these species that appear highly dependent on specific environmental conditions.

57

58 **Introduction**

59 It is increasingly recognized that metabolites produced by the resident microbiota of the
60 colon have a major influence on host physiology (1). Dietary substrates dramatically influence
61 the amount and type of these metabolites produced (2). For instance, fermentation of
62 carbohydrates produces a number of bioactive compounds, most notably short chain fatty acids
63 (SCFA) such as butyrate, that have been demonstrated to shape the gut microenvironment, serve
64 as an energy source for the colonic epithelium, and influence disease through anti-inflammatory,
65 lipogenic, and anti-apoptotic effects (3–6).

66 The production of metabolites in a microbial community has been suggested to be
67 heavily modulated by interactions among its members. These interactions manifest in a variety of
68 modes, ranging from competitive or predatory to commensal and mutualistic exchanges (7).
69 Additionally, many microbes in nature exist in spatially defined structures (8), such as the
70 mucosal layer of the gut. Spatial assortment of cells creates locally heterogeneous
71 subpopulations with varying access to resources that can also modulate inter- and intra-
72 community behavior (9). A major goal of ongoing efforts in human microbiome research (10) is
73 to gain enough predictive and quantitative understanding of inter-microbial interactions (11) and
74 of the metabolic interplay between microbiota and host (12) to be able to understand the effects
75 of the microbiome on human health. These capabilities could greatly facilitate successful design
76 of therapeutic strategies for microbiome-related diseases.

77 Efforts towards safely, effectively and reliably engineering microbial communities (9)
78 to improve human health are, however, limited by insufficient understanding of the nature of the
79 mechanisms underlying microbial interactions and the way these interactions affect microbiome
80 dynamics. Anaerobic *in vitro*, *in vivo* and *ex vivo* experiments capable of probing systems similar
81 to the human colonic environment are difficult and expensive. Previous work uncovering
82 fundamental properties of SCFA-producing bacteria and their symbiotic partners has used
83 *Faecalibacterium prausnitzii* as a model system (13–21). This is motivated by the high
84 prevalence of *F. prausnitzii* as a commensal bacterium in the human large intestine (22) and the
85 role it plays as one of the major butyrate producers (23). Among the bacteria used for coculture
86 studies, a common gut commensal, *Bacteroides thetaiotaomicron*, has been chosen in both
87 experimental (24) and computational (25) analyses of SCFA production. In particular,
88 experimental efforts to grow *F. prausnitzii* in coculture with *B. thetaiotaomicron* have suggested

89 enhancement of butyrate production in coculture relative to *F. prausnitzii* monoculture (24).
90 However, the data in this study was obtained only for a single time point and no information on
91 the dynamics of the biomass or butyrate production was provided. In general, to our knowledge,
92 no comparison has been previously made between experimentally measured time-courses of the
93 biomass of these species and their respective metabolic dynamics, when grown individually and
94 in co-culture.

95 In parallel, computational work based on metabolic network analyses has led to the
96 construction of genome scale models for each of these bacterial species, and to a computational
97 assessment of their metabolic capabilities (26–28). The modeling approach used in these studies,
98 often referred to as constraint-based modeling (or stoichiometric modeling) is based on
99 simplifying assumptions about the intracellular dynamics of metabolism. It enables quantitative
100 predictions of the intracellular and exchange fluxes, in addition to the growth rate of different
101 species. In particular, flux balance analysis (FBA) (29), can be used to calculate the flow of
102 metabolites through a metabolic network, making it possible to predict the growth rate of an
103 organism or the rate of production of important metabolites (30) (see also (31) for a
104 comprehensive review of different approaches). While the reconstructed networks and the
105 modeling tools used for making these predictions vary widely in accuracy and predictive power,
106 the formal representation of metabolism into these mathematical structures and codification of
107 multi-level processes into algorithms have sparked a revolution in systems biology of
108 metabolism, enabling precise hypothesis testing, and the formulation of genome-scale based
109 community modeling. In the context of human gut microbiome studies and inter-species
110 interactions, modeling work has been shown in particular to provide insight into the stability of
111 biofilm forming communities (25).

112 In order to make comparisons between computational predictions and experimental
113 time-course data, it is important to be able to connect detailed knowledge of the intracellular
114 metabolism of individual organisms to the dynamic metabolic changes occurring in the
115 surrounding environment. An extension of FBA capable of these types of calculations is
116 dynamic FBA (or dFBA)(32). Harcombe *et al.* (33) developed a computational framework
117 specifically designed to help predict the spatio-temporal behavior of synthetic microbial
118 consortia. This system, known as Computation of Microbial Ecosystems in Time and Space
119 (COMETS) (33), generates predictions of biomass growth curves as well as detailed time
120 dynamics of the concentrations of all nutrients and metabolites in the environment. COMETS
121 has been shown to accurately predict the behavior of small artificial ecosystems.

122 Despite the availability of these experimental data and computational tools, many
123 fundamental features of the interactions between *F. prausnitzii* and *B. thetaiotaomicron*, as well
124 as our capacity to predict clinically relevant variables, remain unexplored. While previous
125 studies have computationally and experimentally analyzed the metabolic capabilities of each of
126 these bacteria individually (26, 27) and the dependence of these and other bacteria upon different
127 oxygen levels (25), no direct comparison of experimental and computational time course data for
128 this consortium under varying conditions has been presented before. In particular, no attempt
129 has been made to recapitulate or predict these time-courses with dynamic computational models.

130
131 Here, we provide novel insight into the *F. prausnitzii* - *B. thetaiotaomicron* model
132 system by combining new experimental measurements of bacterial biomass and environmental
133 metabolites with COMETS-based computer simulations. We performed a series of anaerobic *in*
134 *vitro* experiments involving monocultures and cocultures of *F. prausnitzii* and *B.*
135 *thetaiotaomicron* grown in three different media, and found increased butyrate production in co-

136 culture relative to monoculture under high glucose and acetate concentrations. Upon fitting of six
137 parameters for metabolic uptake kinetics in monoculture, COMETS simulations were able to
138 recapitulate biomass time courses in monoculture and predict combined biomass time courses for
139 coculture. Model predictions for butyrate, however, portray a more complex picture. Accurate
140 predictions of initial butyrate production rate do not hold at longer times due to the existence of
141 multiple alternative optima in the flux states and the history-dependence of the dynamical
142 predictions. Strong sensitivity of the butyrate production curves to specific concentrations of
143 nutrients, including phosphate, provide insight into the complexity of these metabolic exchanges,
144 and valuable guidance for future experimental and modeling work.

145

146 **Results**

147 ***In vitro* and *in silico* coculture biomass dynamics under different nutrient limitations**

148 We initially characterized anaerobic growth of *B. thetaiotaomicron* and *F. prausnitzii*
149 individually and in coculture, under different levels of carbon availability (low, medium, high,
150 see Methods). In addition to glucose, acetate was added proportionally, mimicking the
151 fermentative activity of the rest of the microbiota (13). The presence of acetate in the medium
152 also allowed us to assess how, even in the absence of *B. thetaiotaomicron*, *F. prausnitzii*
153 responds to varying acetate availability.

154 Monoculture growth for *B. thetaiotaomicron* appears sensitive to the amount of carbon
155 provided (Fig. 1). Growth rate and yield increase in medium acetate/glucose medium compared
156 to low acetate/glucose concentrations. No clear increase in biomass occurred when carbon
157 abundance was increased from medium to high levels. The amount of *F. prausnitzii* biomass in
158 monoculture appears insensitive to increase in initial acetate/glucose levels. The combined

159 biomass growth curves of the coculture (measured as a collective OD) closely tracks OD curves
160 of *B. thetaiotaomicron*, suggesting a prominent role of this bacterium in the consortium. This
161 observation is consistent with previous experiments (3) in which the combined coculture biomass
162 OD of *B. adolescentis* and *F. prausnitzii* mirrors the OD of the *B. adolescentis* monoculture,
163 suggesting that some features of that consortium may be similar to the one studied here, even
164 across different spatial scales and environmental settings.

165 In parallel to the experimental measurements, we implemented *in silico* simulations of
166 the same monocultures and cocultures, using previously published genome-scale metabolic
167 models for the two bacteria (26, 27). In particular, we used COMETS (33) to test whether (i)
168 parameters from the literature, combined with minimal fitting of unknown parameters, would
169 recapitulate the observed monoculture behavior and (ii) models tuned for monoculture
170 experiments would be adequate to predict the outcome of the coculture experiment.

171 Superimposed on the experimental data, Fig. 1 shows the biomass dynamics as
172 simulated in COMETS. The monoculture simulations were supplemented with empirical
173 knowledge of uptake K_M and fitting of V_{max} values. After selecting initial kinetic parameter
174 values based on previously determined corresponding parameters for the phosphotransferase
175 (PTS) transporter (21, 34), a sensitivity analysis allowed us to identify V_{max} values that provide
176 best fit of growth curves to monoculture (Fig. 2). This calibration step, similar to that previously
177 performed in (35), produces simulated OD curves that broadly agree with the experimentally
178 measured points (see root-mean-squared error (RMSE) in Table 1). Using these parameters for
179 COMETS simulations of cocultures at the experimentally estimated initial biomass abundances,
180 coculture predictions track coculture experimental data closely, as shown by predictive RMSE
181 values (Table 1).

182

183 **Coculture conditions impact the average rate of butyrate production in experiments**

184 Throughout all of our experiments, in addition to monitoring the overall OD, we
185 measured the extracellular abundance of butyrate and acetate. In Fig. 3, the average amount of
186 butyrate produced by *F. prausnitzii* in coculture appears higher than monoculture in the medium
187 and high initial acetate/glucose concentrations, but not in the low concentration conditions. In
188 low acetate/glucose conditions the butyrate production rate in coculture appears suppressed
189 relative to the one in monoculture. Box's approach in (36), applying ANOVA to summary
190 statistics describing growth curves, was used to quantify the statistical significance of the
191 difference in butyrate production curves across different treatments, i.e.: (i) monoculture vs.
192 coculture conditions (mono/co) and (ii) the three different initial acetate/glucose initial
193 concentrations (initial glu/ac). Tables 2 and 3 show that the average rate of butyrate production
194 in *F. prausnitzii* is significantly altered in mono vs. coculture conditions but not across the
195 different initial abundances of acetate and glucose. The initial acetate/glucose concentrations, but
196 not mono vs. coculture conditions, significantly change the average rate of acetate production
197 from *B. thetaiotaomicron*.

198 Interpretation of the above assessments of butyrate and acetate production is limited by
199 the lack of experimental knowledge of the precise amount of biomass of each species in the
200 coculture experiments. In particular, in absence of further laborious organism-specific data, it is
201 impossible to determine whether significant changes in the level of the butyrate curves are due to
202 *F. prausnitzii* producing more butyrate at the cellular level in the coculture, or whether the
203 increase is due to an increase in *F. prausnitzii* total biomass, enabled by coculture conditions, or
204 both. Under these circumstances, COMETS-predicted biomass estimates for each species from

205 coculture simulations (Fig. 6B) enabled hybrid computational-experimental estimates of
206 biomass-normalized butyrate (Fig. 6A) and acetate (Fig. S2) production curves.

207 Trends of significance in Tables 5 and 6 for the normalized curves are similar to those
208 for the unnormalized curves, with several exceptions. The average rate of both SCFAs are
209 significantly affected by mono vs. coculture conditions in the normalized curves. These results
210 imply that *B. thetaiotaomicron* stimulates butyrate production in *F. prausnitzii* on a per cell basis
211 rather than by stimulating *F. prausnitzii* biomass production. *B. thetaiotaomicron* biomass-
212 normalized acetate production curves are not significantly changed in average rate by initial
213 glucose/acetate levels, in contrast to the non-normalized curves. As a note of caution, it is
214 important to stress that the normalization relative to untested predicted abundances of individual
215 species in co-culture should be considered putative. At the same time, it could be viewed as a
216 valuable strategy for integrating experimental and computational data towards the formulation of
217 new hypotheses.

218

219 **The multiplicity of fermentation states with optimal efficiency influences SCFA time-course** 220 **predictability**

221 Figure 3 shows that COMETS accurately recapitulates the early stages of
222 accumulation of extracellular butyrate. After 5 hours of growth, however, the picture becomes
223 more complex. Simulation results at these times suggest that the regulation of butyrate and
224 lactate pathways may play a major role in the final outcome of the secreted butyrate. To
225 understand these results, the butyrate fermentation process in *F. prausnitzii* was revisited with
226 additional computational analyses, specifically focused on alternative fermentation pathways.
227 Three competing fermentation pathways exist in the curated metabolic network of *F. prausnitzii*.
228 Pyruvate is fermented to one of the three products (27): (i) lactate, by D-lactate dehydrogenase

229 (reaction ID: LDH_D), (ii) formate, by pyruvate-formate lyase (reaction ID: PFL) or (iii) butyrate,
230 by butyryl-CoA:acetate CoA-transferase (reaction ID: BTCOAACCOAT). Butyryl-CoA in turn
231 is produced from acetyl-CoA (reaction ID: BTCOADH) and acetyl-CoA is converted from
232 pyruvate by pyruvate:ferredoxin oxidoreductase (reaction ID: POR4i). The balance of metabolic
233 flow through these three closely coupled fermentation pathways can significantly impact the
234 production of butyrate in *F. prausnitzii*, depending on environmental conditions.

235 As shown in Figs. 3 and S4, and described in the methods section, COMETS, in its
236 standard formulation, switches among these competing pathways. In particular, Figure S3 shows
237 that *F. prausnitzii* switches from predominantly butyrate production activity at time zero to
238 lactate secretion after 5 hours. This switch coincides with the transition from a single solution
239 point of the FBA optimization at the early stages of the growth, to conditions where the FBA
240 optimization algorithm has the freedom of choosing between a multitude of flux solution points,
241 all corresponding to the same biomass growth rate. This multiplicity of equivalently efficient
242 steady states (multiple alternative optima, also described in (37)) is best highlighted by
243 systematically imposing, at each time point, additional features in the dFBA solution process. In
244 particular, in analogy with flux variability analysis (38), we re-run the COMETS simulations by
245 adding a secondary objective function at each time point. After maximizing for growth, the
246 algorithm fixes the growth rate to the identified maximum, and subsequently searches for the
247 solution that maximizes or minimizes the secretion flux of one of the organic acids, such as
248 butyrate. Correspondingly, the butyrate secretion flux can be represented in the form of two
249 curves of butyrate concentration extremes (Fig. 3). Notably, in most of the cases, the
250 experimentally measured butyrate concentrations occupy a place between these two extremes.
251 Nutrient limitations seem to be a strong determinant of this multiplicity of alternative optima.

252 The system is particularly sensitive to phosphate concentration, as shown in Figs. 4 and S4, and
253 is probably due to the strong coupling to phosphate in all butyrate producing pathways. These
254 simulation results therefore suggest that regulation of the fermentation pathways in *F. prausnitzii*
255 influence butyrate production under different environmental conditions.

256 The simulated acetate production shown in Fig. 5 tracks experimental time courses for
257 both *B. thetaiotaomicron* and *F. prausnitzii* monoculture, particularly in the medium and high
258 initial acetate/glucose conditions. Simulated time courses fall within error bars for average
259 experimental observations for all time points on the curves. The early stages of the coculture
260 simulations also closely track experiments. After 5 simulated hours, however, opposite trends in
261 acetate concentrations appear to mirror the discrepancies with experiment in the butyrate
262 simulations. While the experiments show depletion, the simulations result in buildup of acetate
263 in the late stages of the simulations. This inconsistency is also potentially explainable by a
264 metabolic switch in *F. prausnitzii*, resulting in less acetate consumption to produce butyrate.

265

266 **Discussion**

267 We analyzed experimentally and computationally the possible effects of a symbiotic
268 partner (*B. thetaiotaomicron*) and of environmental conditions (amount of glucose and acetate)
269 on the biomass of the gut bacterium *F. prausnitzii*, as well as its capacity to produce butyrate. In
270 monoculture, *F. prausnitzii* seems to continue producing butyrate even after the cells reach
271 stationary phase (at around 10 hours), suggesting that maintenance processes keep fueling the
272 butyrate production pathways. Another feature of the monoculture is the relatively low
273 sensitivity of biomass and butyrate production to glucose and acetate concentrations. In contrast,
274 biomass and butyrate seem to more strongly depend on the environment in the presence of *B.*

275 *thetaitotaomicron* in the coculture experiments (Figure 3), although this difference is not
276 statistically significant, based on ANOVA.

277 The possibility of metabolic cross-feeding between *F. prausnitzii* and *B.*
278 *thetaitotaomicron* has been suggested in previous studies (24). In some of these studies, acetate
279 production by *B. thetaitotaomicron* is proposed to mediate the interaction between the two
280 bacteria, facilitating an increased butyrate production by *F. prausnitzii*. While it is likely that
281 indeed acetate plays a key role in the interaction between the two bacteria, the results of our
282 study suggest a more complex mode of interaction: First, the statistically significant increase in
283 butyrate production we observe in coculture does not seem to increase monotonically with the
284 amount of glucose and acetate, suggesting that either the two carbon sources are saturated (24),
285 or that acetate exchange is not the only factor dominating butyrate production. Second, as
286 demonstrated by our COMETS dFBA simulations, the stoichiometry of *F. prausnitzii* suggests
287 that multiple alternative growth optima are possible (depending on whether or not other nutrients
288 – most notably phosphate – are limiting in the medium). These different optima can differ
289 substantially in their combination of fermentation products, thus making the stoichiometry-based
290 prediction of a specific rate of butyrate production impossible. Instead, only a range of
291 production rates can be predicted at any given time. This hypothesized degree of freedom in
292 fermentative pathways could in principle be used by *F. prausnitzii* to modulate its metabolic
293 activity and its butyrate production rate in response to external signals. Future studies using
294 dFBA for studying *F. prausnitzii* could use additional constraints (e.g. total flux capacity (38) or

295 regulatory information (38)) to refine the predictions, and to systematically test the effect of
296 different nutrient limitations and growth media on butyrate production.

297 In this work, COMETS predictions were also used to estimate relative biomass amount
298 of the two species in coculture, in the absence of experimental observations. Although the
299 accuracy of the COMETS relative biomass estimates were not confirmed using experimental
300 data, its ability to predict the total biomass in coculture using parameters learned from
301 monoculture conditions lends credence to these estimates. Follow-up experiments to fully vet
302 model accuracy in determining relative biomass in consortia would be invaluable towards
303 building confidence in hybrid computational-experimental approaches like the one demonstrated
304 here.

305

306 **Methods and Materials**

307 ***COMETS Simulation Configuration*** The metabolic network models we use in this work for
308 *Bacteroides thetaiotaomicron* strain VPI-5482 and *Faecalibacterium prausnitzii* strain A2-165
309 were published and made publicly available by Heinken *et al.* in (26) and (27). The COMETS
310 simulation framework is implemented in Java and described in (33). R and Matlab scripts
311 transform COMETS outputs to time-course plots. The 3D volume in these simulations contains 5
312 mL of isotropic medium and biomass. COMETS' ability to model spatial differences in
313 microbial systems is not explored in these preliminary simulations. Similarly, the dFBA settings,
314 other than the ones mentioned below, were set at their default values as implemented in
315 COMETS. The FBA parsimonious optimization was performed using the GUROBI optimizer,
316 with a primary maximization of the biomass growth rate and a secondary minimization of the
317 absolute values sum of the metabolic fluxes. The butyrate secretion analysis also included

318 additional maximization and/or minimization of butyrate, lactate and formate uptake. Simulation
319 run time was 24 hours, with each time step set to 0.01 hour. The death rate was set to zero.

320 The uptake of nutrients was modeled as a saturation Michaelis-Menten curve with two
321 adjustable parameters, maximum uptake flux, V_{\max} , and the Michaelis constant K_M . Our choice
322 of parameters for the uptake curve was guided by values provided in the original publications of
323 the models and as reported in the literature (39, 40). The glucose uptake in *F. prausnitzii*, for
324 example, is governed by PTS transporter (27) with reported K_M values up to 8.7 mM (34). These
325 starting values for the uptake parameters were additionally fine-tuned by fitting the single-
326 species simulations results for the OD to the corresponding experimental curves. **Error!**
327 **Reference source not found.** shows the fitting procedure for *B. thetaiotaomicron* and *F.*
328 *prausnitzii* respectively. In the case of *B. thetaiotaomicron* a single value for the maximum
329 uptake parameter was sufficient to fit the growth curves. The accepted value minimized the
330 composite reduced chi-squared for all three growth conditions. In the case of *F. prausnitzii*, we
331 used two values for the maximum uptake. Starting with the value for K_M we fitted the glucose
332 and acetate uptake, and then performed a fine tuning for the rest of the metabolites/nutrients.
333 Parameter values are shown in Table 6.

334 Metabolic activity in the *F. prausnitzii* model showed a nutrient concentration
335 dependent shift, most sensitive to phosphate depletion, from butyrate producing pathway, to a
336 lactate producing one, shown in Fig. S3. This shift is characterized by a single solution point of
337 the FBA optimization sequence, both for minimized and maximized butyrate secretion, at high
338 values of phosphate concentration, shown in Fig. S4, corresponding to the initial time in the
339 dFBA simulation. As the substrate is depleted of the nutrients, the system obtains multiple
340 optimal solution points, with the difference in the butyrate production depending on the

341 secondary optimization of butyrate secretion (Fig. S4) providing a range of possible butyrate
342 secretion rates at the later stages of the dFBA simulations. The complete set of input as well as
343 simulations output files can be found in the supplement. COMETS is available to download at
344 comets.bu.edu.

345
346 ***ANOVA Methodology*** Box's method (36) for describing and quantifying differences in growth
347 curves was implemented as follows. The average rate/level statistic is computed as the average
348 of the measurements from the first time point concentration measurement subtracted from the
349 average of the measurements from the last divided by the total time. The rate of butyrate
350 production for each time bin was computed similarly and the average rate was subtracted from
351 these for the set of rate deviations that define the shape statistic.

352 We use the Bonferonni corrected significance level of 0.0042 in this study with twelve
353 comparisons (six per metabolite) to conservatively approximate the 0.05 significance level in
354 single comparisons. The small number of replicates in our study (3 replicates), results in
355 relatively low power for ANOVA tests. Insignificant results in our ANOVA analysis may
356 therefore derive from low power, randomness or some combination of the two (41) for both the
357 *shape* and *level* ANOVA results. Additionally, violations of homogeneous measurement
358 covariance matrices and/or normally distributed prediction errors with zero mean could also
359 result in pessimistically biased significance estimates. In particular, violation of homogeneous
360 covariance matrices may negatively bias *shape* ANOVA results (42). ANOVA results for *level*
361 have been shown to be robust to violations of this assumption (43).

362 We did not test our data for violations of these two conditions because tests for normality
363 and equal variance are themselves inconclusive with small sample sizes. Given that violations of

364 homogeneous measurement covariance matrices can negatively bias significance results in *shape*
365 ANOVA, the insignificant results in this study should be probed further with larger sample sizes.
366 Because *level* ANOVA results have been shown to be robust to violations of homogeneous
367 measurement covariance matrices (43), we are confident in the finding of significant differences
368 between monoculture and coculture metabolite production curves in *level*/average rate. As is
369 always the case, however, follow-up studies with larger sample sizes would be advised to both
370 test reproducibility and lend more power to ANOVA results.

371
372 ***In Vitro Experimental Configuration/OD600 Analysis*** Bacteria were cultured in Yeast
373 Casitone (YC) medium, with three different concentrations of supplemented acetic acid/glucose.
374 “Low” condition: 5.551mM acetic acid, .1% glucose. “Medium” condition: 27.754mM acetic
375 acid, .5% glucose. “High” condition: 55.507mM acetic acid, 1% glucose. All media were
376 adjusted to pH 6.8 before autoclaving.

377 Bacterial cultures were started in anaerobic conditions from glycerol stocks stored at -
378 80°C in 3mL of “Medium” YC medium. After overnight culture, OD600 was measured, and the
379 cultures were diluted to the nominal OD starting points in 5mL of the three different YC
380 formulations.

381 The following cultures were started with the initial OD600 values as noted:

382 OD600 ~.02 *B. thetaiotamicron* monoculture

383 OD600 ~.08 *F. prausnitzii* monoculture

384 OD600 ~.02 *B. thetaiotamicron* AND OD600 ~.08 *F. prausnitzii* coculture

385 A baseline 200µL aliquot was taken from each culture, measured by OD600, and stored
386 at -80 for later MS analysis. Subsequent 200µL aliquots were collected and measured by OD600

387 at 2, 4, 6, 8, 10 and 24 hours and stored for later analysis. The above procedure was repeated in
388 triplicate, yielding three observations per time point.

389
390 **MSMS Analysis** A flow injection analysis electrospray ionization mass spectrometry (FIA ESI
391 MSMS) method was used for quantitative detection of short chain fatty acids (SCFA). Acetic,
392 propionic, butyric and succinic acid were derivatized with 3-nitrophenylhydrazine in the
393 presence of N-(3-dimethylaminopropyl)-N'-ethylcarbodiimide and pyridine and detected by a
394 mass spectrometer as a 3-nitrophenylhydrozones in MRM (multiple reaction monitoring) MSMS
395 mode, as described by J. Han *et al.* (44). To increase precision and robustness of the method, 3-
396 methylbutyric-2-2-d₂ acid, acetic acid-2-13C and propionic acid -1-13C were used as an
397 internal standards. Quantitation was done by external standards calibration, where instrument
398 response for the analyte was measured as a ratio between analyte's and internal standard's peak
399 areas. The FIA technique did not utilize LC column but rather a direct injection of the sample
400 into an ESI probe of the mass spectrometer and this decreased time of analysis per sample to two
401 minutes. The FIA ESI MSMS for the detection of SCFA is sensitive with the limit of detection
402 for acetic, propionic, butyric and succinic acids at 4, 3, 0.6 and 1.4 μM respectively. The
403 accuracy of the method was between 98-102%.

404
405 **Reagents** LC MS grade acetonitrile and water were purchased from VWR (Radnor, PA, USA).
406 N-(3-dimethylaminopropyl)-N'-ethylcarbodiimide HCl, 3-nitrophenylhydrazine HCl, pyridine,
407 acetic acid, propionic acid, butyric acid, succinic acid, acetic acid 13C, and propionic acid 13C
408 were purchased from Sigma-Aldrich (St Luis, MO, USA). 3-methylbutyric-2-2-d₂ acid was
409 purchased from CDN Isotopes (Quebec, CN).

410
411 **FIA MS/MS system** An Agilent infinity capillary LC pump with micro-autosampler and
412 thermostat (Agilent Technologies, Santa Clara, CA, USA) coupled to AB Sciex 4000 Q-TRAP
413 triple- quadrupole mass spectrometer (AB Sciex, Concord, Ontario, CN) was used for the
414 analysis. The flow solvent - five percent water and ninety five percent acetonitrile was delivered
415 to a mass spectrometer ESI probe at the rate of 350 μ L/min. Samples for flow injection analysis
416 were derivatized on the Agilent polypropylene 96 well plate and injected into mass spectrometer
417 with injection volume of 40 μ L. Following conditions for the AB Sciex Q-TRAP 4000 were used
418 for analysis: source temperature 400°C, source gas 40L/min, curtain gas 10L/min, ESI capillary
419 voltage was set at -4500 volts. Data were acquired in negative polarity multiple reactions
420 monitoring (MRM) mode for the MRM transitions specified in the Table S1.

421
422 **Data Availability**
423 Data files and scripts used to generate the figures presented in this paper can be found in a zipped
424 directory (Yu_etal_Data_and_Scripts.zip) downloadable at [https://github.com/segrelab/Fprau-](https://github.com/segrelab/Fprau-Btheta-2018)
425 [Btheta-2018](https://github.com/segrelab/Fprau-Btheta-2018). This directory contains the experimental data and script for statistical analysis and
426 for generating the figures (DATA_AND_FIGURE_SCRIPTS subdirectory), and COMETS input
427 and output files (SIMULATIONS_INPUTS_AND_OUTPUTS subditrectory). The *in silico*
428 experiments were generated using COMETS v.2.5.8, which is freely available at
429 <http://comets.bu.edu>.

430
431 **Acknowledgements**

432 DS and ID acknowledge funding from the Defense Advanced Research Projects Agency
433 (Purchase Request No. HR0011515303, Contract No. HR0011-15-C-0091), the NIH
434 (5R01DE024468, R01GM121950 and Sub_P30DK036836_P&F), and the Boston University
435 Interdisciplinary Biomedical Research Office. This material is based upon work supported by
436 the Assistant Secretary of Defense for Research and Engineering under Air Force Contract No.
437 FA8702-15-D-0001. Any opinions, findings, conclusions or recommendations expressed in this
438 material are those of the author(s) and do not necessarily reflect the views of the Assistant
439 Secretary of Defense for Research and Engineering.

440
441 **References**

- 442 1. Lozupone CA, Stombaugh JI, Gordon JI, Jansson JK, Knight R. 2012. Diversity, stability
443 and resilience of the human gut microbiota. *Nature* 489:220–230.
- 444 2. Yatsunencko T, Rey FE, Manary MJ, Trehan I, Dominguez-Bello MG, Contreras M,
445 Magris M, Hidalgo G, Baldassano RN, Anokhin AP, Heath AC, Warner B, Reeder J,
446 Kuczynski J, Caporaso JG, Lozupone CA, Lauber C, Clemente JC, Knights D, Knight R,
447 Gordon JI. 2012. Human gut microbiome viewed across age and geography. *Nature*
448 486:222–227.
- 449 3. Rios-Covian D, Gueimonde M, Duncan SH, Flint HJ, De Los Reyes-Gavilan CG. 2015.
450 Enhanced butyrate formation by cross-feeding between *Faecalibacterium prausnitzii* and
451 *Bifidobacterium adolescentis*. *FEMS Microbiol Lett* 362:1–7.
- 452 4. Canani RB, Costanzo M Di, Leone L, Pedata M, Meli R, Calignano A. 2011. Potential
453 beneficial effects of butyrate in intestinal and extraintestinal diseases. *World J*
454 *Gastroenterol* 17:1519–1528.
- 455 5. Flint HJ, Duncan SH, Scott KP, Louis P. 2015. Links between diet, gut microbiota

- 456 composition and gut metabolism. *Proc Nutr Soc* 74:13–22.
- 457 6. Lopez-Siles M, Khan TM, Duncan SH, Harmsen HJM, Garcia-Gil LJ, Flint HJ. 2012.
458 Cultured representatives of two major phylogroups of human colonic *Faecalibacterium*
459 *prausnitzii* can utilize pectin, uronic acids, and host-derived substrates for growth. *Appl*
460 *Environ Microbiol* 78:420–428.
- 461 7. Mitri S, Richard Foster K. 2013. The Genotypic View of Social Interactions in Microbial
462 Communities. *Annu Rev Genet* 47:247–273.
- 463 8. Kolter R, Greenberg EP. 2006. Microbial sciences: The superficial life of microbes.
464 *Nature* 441:300–302.
- 465 9. Johns NI, Blazejewski T, Gomes ALC, Wang HH. 2016. Principles for designing
466 synthetic microbial communities. *Curr Opin Microbiol* 31:146–153.
- 467 10. Turnbaugh PJ, Ley RE, Hamady M, Fraser-Liggett CM, Knight R, Gordon JI. 2007. The
468 Human Microbiome Project. *Nature* 449:804–810.
- 469 11. Venturelli OS, Carr AC, Fisher G, Hsu RH, Lau R, Bowen BP, Hromada S, Northen T,
470 Arkin AP. 2018. Deciphering microbial interactions in synthetic human gut microbiome
471 communities. *Mol Syst Biol* 14:e8157.
- 472 12. Nicholson JK, Holmes E, Kinross J, Burcelin R, Gibson G, Jia W, Pettersson S. 2012.
473 *Metabolic Interactions* 108:1262–1268.
- 474 13. Belzer C, Chia LW, Aalvink S, Chamlagain B, Piironen V, Knol J, de Vos WM. 2017.
475 Microbial metabolic networks at the mucus layer lead to diet-independent butyrate and
476 vitamin B12 production by intestinal symbionts. *MBio* 8:1–14.
- 477 14. Das P, Ji B, Kovatcheva-Datchary P, Bäckhed F, Nielsen J. 2018. In vitro co-cultures of
478 human gut bacterial species as predicted from co-occurrence network analysis. *PLoS One*

- 479 13:1–14.
- 480 15. Duncan SH, Barcenilla A, Stewart CS, Pryde SE, Flint HJ. 2002. Acetate utilization and
481 butyryl coenzyme A (CoA): Acetate-CoA transferase in butyrate-producing bacteria from
482 the human large intestine. *Appl Environ Microbiol* 68:5186–5190.
- 483 16. Louis P, Flint HJ. 2009. Diversity, metabolism and microbial ecology of butyrate-
484 producing bacteria from the human large intestine. *FEMS Microbiol Lett* 294:1–8.
- 485 17. Miquel S, Martin R, Bridonneau C, Robert V, Sokol H, Bermúdez-Humarán LG, Thomas
486 M, Langella P. 2014. Ecology and metabolism of the beneficial intestinal commensal
487 bacterium *Faecalibacterium prausnitzii*. *Gut Microbes* 5.
- 488 18. PrévotEAU A, Geirnaert A, Arends JBA, Lannebère S, Van De Wiele T, Rabaey K. 2015.
489 Hydrodynamic chronoamperometry for probing kinetics of anaerobic microbial
490 metabolism - Case study of *Faecalibacterium prausnitzii*. *Sci Rep* 5:1–13.
- 491 19. Sokol H, Pigneur B, Watterlot L, Lakhdari O, Bermudez-Humaran LG, Gratadoux J-J,
492 Blugeon S, Bridonneau C, Furet J-P, Corthier G, Grangette C, Vasquez N, Pochart P,
493 Trugnan G, Thomas G, Blottiere HM, Dore J, Marteau P, Seksik P, Langella P. 2008.
494 *Faecalibacterium prausnitzii* is an anti-inflammatory commensal bacterium identified by
495 gut microbiota analysis of Crohn disease patients. *Proc Natl Acad Sci* 105:16731–16736.
- 496 20. Tremaroli V, Bäckhed F. 2012. Functional interactions between the gut microbiota and
497 host metabolism. *Nature* 489:242–249.
- 498 21. Stewart CS, Hold GL, Duncan SH, Flint HJ, Harmsen HJM, Hold GL, Harmsen HJM,
499 Stewart CS, Flint HJ. 2002. Growth requirements and fermentation products of
500 *Fusobacterium prausnitzii*, and a proposal to reclassify it as *Faecalibacterium prausnitzii*
501 gen. nov., comb. nov. *Int J Syst Evol Microbiol* 52:2141–2146.

- 502 22. Maier, Eva. 2017. Effect of *Faecalibacterium prausnitzii* on intestinal barrier function and
503 immune homeostasis.
- 504 23. Vital M, Karch A, Pieper DH. 2017. Colonic Butyrate-Producing Communities in
505 Humans: an Overview Using Omics Data. *mSystems* 2:e00130-17.
- 506 24. Wrzosek L, Miquel S, Noordine ML, Bouet S, Chevalier-Curt MJ, Robert V, Philippe C,
507 Bridonneau C, Cherbuy C, Robbe-Masselot C, Langella P, Thomas M. 2013. *Bacteroides*
508 *thetaiotaomicron* and *Faecalibacterium prausnitzii* influence the production of mucus
509 glycans and the development of goblet cells in the colonic epithelium of a gnotobiotic
510 model rodent. *BMC Biol* 11.
- 511 25. Henson M, Phalak P. 2017. Byproduct Cross Feeding and Community Stability in an In
512 Silico Biofilm Model of the Gut Microbiome. *Processes* 5:13.
- 513 26. Heinken A, Sahoo S, Fleming RMT, Thiele I. 2013. Systems-level characterization of a
514 host-microbe metabolic symbiosis in the mammalian gut. *Gut Microbes* 4.
- 515 27. Heinken A, Khan MT, Paglia G, Rodionov DA, Harmsen HJM, Thiele I. 2014. Functional
516 metabolic map of *Faecalibacterium prausnitzii*, a beneficial human gut microbe. *J*
517 *Bacteriol* 196:3289–3302.
- 518 28. El-Semman IE, Karlsson FH, Shoaie S, Nookaew I, Soliman TH, Nielsen J. 2014.
519 Genome-scale metabolic reconstructions of *Bifidobacterium adolescentis* L2-32 and
520 *Faecalibacterium prausnitzii* A2-165 and their interaction. *BMC Syst Biol* 8:1–11.
- 521 29. Orth JD, Thiele I, Palsson BØ. 2010. What is flux balance analysis? *Nat Biotechnol*
522 28:245–8.
- 523 30. Feist AM, Zielinski DC, Orth JD, Schellenberger J, Markus J, Palsson BØ. 2011. Model-
524 driven evaluation of the production potential for growth coupled products of *Escherichia*

- 525 coli. *Metab Eng* 12:173–186.
- 526 31. Zomorodi AR, Segrè D. 2016. Synthetic ecology of microbes: mathematical models and
527 applications Graphical Abstract HHS Public Access. *J Mol Biol J Mol Biol Febr Pt B*
528 27:837–861.
- 529 32. Mahadevan R, Edwards JS, Doyle FJ. 2002. Dynamic Flux Balance Analysis of diauxic
530 growth in *Escherichia coli*. *Biophys J* 83:1331–1340.
- 531 33. Harcombe WR, Riehl WJ, Dukovski I, Granger BR, Betts A, Lang AH, Bonilla G, Kar A,
532 Leiby N, Mehta P, Marx CJ, Segrè D. 2014. Metabolic resource allocation in individual
533 microbes determines ecosystem interactions and spatial dynamics. *Cell Rep* 7:1104–1115.
- 534 34. Castro R, Neves AR, Fonseca LL, Pool WA, Kok J, Kuipers OP, Santos H. 2009.
535 Characterization of the individual glucose uptake systems of *Lactococcus lactis*: Mannose-
536 PTS, cellobiose-PTS and the novel GlcU permease. *Mol Microbiol* 71:795–806.
- 537 35. Louca S, Doebeli M. 2015. Calibration and analysis of genome-based models for
538 microbial ecology. *Elife* 4:1–17.
- 539 36. Box GEP. 1950. Problems in the Analysis of Growth and Yield Curves Author (s): G . E
540 . P . Box Published by : International Biometric Society Stable URL :
541 <http://www.jstor.org/stable/3001781> REFERENCES Linked references are available on
542 JSTOR for this article : You may. *Biometrics* 6:362–389.
- 543 37. Segre D, Vitkup D, Church GM. 2002. Analysis of optimality in natural and perturbed
544 metabolic networks. *Proc Natl Acad Sci* 99:15112–15117.
- 545 38. Mahadevan R, Schilling CH. 2003. The effects of alternate optimal solutions in constraint-
546 based genome-scale metabolic models. *Metab Eng* 5:264–276.
- 547 39. Meadows AL, Karnik R, Lam H, Forestell S, Snedecor B. 2010. Application of dynamic

- 548 flux balance analysis to an industrial *Escherichia coli* fermentation. *Metab Eng* 12:150–
549 160.
- 550 40. Jahreis K, Pimentel-Schmitt EF, Brückner R, Titgemeyer F. 2008. Ins and outs of glucose
551 transport systems in eubacteria. *FEMS Microbiol Rev* 32:891–907.
- 552 41. Hewitt CE, Mitchell N, Torgerson DJ, Hewitt C, Torgerson D. 2008. significant
553 Unexpected non-significant results from randomised trials can be difficult to accept . 23–
554 25.
- 555 42. Snee RD. 1972. American Society for Quality On the Analysis of Response Curve Data
556 On the Analysis of Response Curve Data. Source: *Technometrics* 14:47–62.
- 557 43. Grenhouse, Samuel W. Geisser S. 1959. ON METHODS IN THE ANALYSIS OF
558 PROFILE variance . Furthermore , an analysis of variance approach permits the analysis
559 of a set of data which cannot be handled by multivariate procedures , namely , the case
560 where n , the number of random vectors , is less t. *Psychometrika* 24:95–112.
- 561 44. Han J, Lin K, Sequeira C, Borchers CH. 2015. An isotope-labeled chemical derivatization
562 method for the quantitation of short-chain fatty acids in human feces by liquid
563 chromatography-tandem mass spectrometry. *Anal Chim Acta* 854:86–94.

564

565

566 **Tables:**

567

	Low	Medium	High
Coculture	0.110	0.071	0.049
<i>B. thetaiotaomicron</i>	0.034	0.065	0.112
<i>F. prausnitzii</i>	0.064	0.094	0.043

568
 569 **Table 1.** Table of RMSE between the values in Fig. 1 measured experimentally and predicted by
 570 simulations, for monocultures and coculture in three carbon source conditions as described in the
 571 text.

572
 573

Source	Acetate					Butyrate				
	Sum Sq.	d.f.	Mean Sq.	F	Prob>F	Sum Sq.	d.f.	Mean Sq.	F	Prob>F
initial glc/ac	21.14	2	10.571	0.47	0.6277	1.3206	2	0.66032	0.69	0.5015
mono/co	115.13	1	115.131	5.1	0.0261	0.11956	1	0.11945	0.13	0.7237
initialglc/ac*mono/co	76.86	2	38.43	1.7	0.1877	0.275	2	0.13751	0.14	0.8655
Error	2304.56	102	22.594			96.9437	102	0.95043		
Total	2517.69	107				98.6588	107			

574
 575 **Table 2.** Analysis of Variance of Shape of Metabolite Curves.

576
 577

Source	Acetate					Butyrate				
	Sum Sq.	d.f.	Mean Sq.	F	Prob>F	Sum Sq.	d.f.	Mean Sq.	F	Prob>F
initial glc/ac	20.8263	1	20.8263	17.66	0.0012	0.17635	1	0.17635	4.29	0.0606
mono/co	1.6629	2	0.8315	0.7	0.5135	2.09982	2	1.04991	25.53	0
initialglc/ac*mono/co	13.2214	2	6.6107	5.61	0.0191	0.41137	2	0.20568	5	0.0263
Error	14.1527	12	1.1794			0.49346	12	0.04112		
Total	49.8634	17				3.181	17			

578
 579 **Table 3.** Analysis of Variance of Average Rate of Metabolite Curves.

580
 581

Source	Acetate					Butyrate				
	Sum Sq.	d.f.	Mean Sq.	F	Prob>F	Sum Sq.	d.f.	Mean Sq.	F	Prob>F
initial glc/ac	1.81E+07	2	9.06E+06	0.08	0.9272	2745098	2	1372549	0.46	0.6328
mono/co	4.80E+06	1	4.80E+06	0.04	0.8417	25019.6	1	25019.6	0.01	0.9272
initialglc/ac*mono/co	9.61E+06	2	4.81E+06	0.04	0.9606	953798	2	476899	0.16	0.8526
Error	1.22E+10	102	1.20E+08			3E+08	102	2985539		
Total	1.23E+10	107				3.1E+08	102			

582
 583 **Table 4.** Analysis of Variance of Average Rate of Metabolite Curves.

584

Source	Acetate					Butyrate				
	Sum Sq.	d.f.	Mean Sq.	F	Prob>F	Sum Sq.	d.f.	Mean Sq.	F	Prob>F

Source	Sum Sq.	d.f.	Mean Sq.	F	Prob>F	Sum Sq.	d.f.	Mean Sq.	F	Prob>F
initial glc/ac	162363.1	1	162363.1	1.57	0.234	11506.9	1	11506.9	0.2	0.6612
mono/co	3919429.3	2	1959714.6	18.96	0.0002	1156514	2	578257	10.15	0.0026
initialglc/ac*mono/co	2590821	2	1295410.5	12.53	0.0012	517152	2	258576	5.54	0.0341
Error	12640529.9	12	103377.5			683892	12	56991		
Total	7913143.3	17				2369065	17			

585
586 **Table 5.** Analysis of Variance of Average Rate of Biomass-Normalized Metabolite Curves.

587

Species	V_{max} [mmol/hg]	Glc./Ac. V_{max} [mmol/hg]	K_m [mM]	Glc./Ac. K_m [mM]
<i>B.thetaiotaomicoron</i>	11	11	3	3
<i>F. prausnitzii</i>	23	10	10	5

588
589 **Table 6.** Parameters of the Michaelis-Menten uptake functions. Glucose and acetate uptake
590 parameters were obtained independently from the rest of the nutrients for the model of *F.*
591 *prausnitzii*.

592

593 **Supplemental table legend:**

594 Table S1. AB Sciex 4000-TRAP parameters used for detection of SCFA Q1 – m/z of the analyte
595 ion detected on the 1st quadrupole. Q3 – m/z of the analyte's fragment ion detected on the third
596 quadrupole. DP- declustering potential, CE – collision energy. Analytes in red are internal
597 standards.

598

599 **Figure legends:**

600 **Figure 1.** Optical densities for single species and coculture of *F. prausnitzii* and *B.*
601 *thetaiotaomicron*, grown in three different media conditions. The simulations (solid curves) were

602 obtained by dFBA with the same set of uptake parameters for all media conditions. The columns
603 correspond to the media conditions while the rows correspond to the cultured species.

604

605 **Figure 2.** The sensitivity of the OD curves to the values of the maximum nutrient uptake
606 parameter V_{max} . The values of the V_{max} parameter used in the simulations were obtained by
607 minimizing χ^2 , the sum of the squared deviations of the simulation from the experimental values,
608 weighted by the measured variance. We used a single value of V_{max} for the uptake of all
609 nutrients by the *B. thetaiotaomicron* model, with the minimum of minimizing χ^2 , shown in panel
610 A). In the case of *F. prausnitzii*, we determined two separate values of minimizing χ^2 , one for
611 glucose and acetate uptake shown on panel B), and another one for the rest of the nutrients,
612 shown on panel C).

613

614 **Figure 3.** Experimental and simulated (solid, dot and dash curves) butyrate production
615 time courses for monocultures and coculture under the three initial glucose/acetate initial
616 concentrations. Apparent differences demonstrated in these plots in butyrate production for *F.*
617 *prausnitzii* monoculture vs. coculture and for the three initial concentrations can be tested
618 statistically using ANOVA on summary statistics describing the curves. The simulated curves
619 correspond to the maximized (solid curve) and minimized (dash dot curve) butyrate secretion.

620

621 **Figure 4.** Simulated butyrate production for three starting abundances of phosphate for
622 the low initial acetate/glucose concentration. Lowering of the phosphate concentration leads to
623 multiple FBA solutions and difference between secondary minimization and maximization of
624 butyrate secretion.

625

626 **Figure 5.** Experimental and simulated (solid curves) acetate production time courses for

627 monocultures and coculture under the three initial glucose/acetate initial concentrations.

628 Apparent differences demonstrated in these plots in butyrate production for *F. prausnitzii*

629 monoculture vs. coculture and for the three initial concentrations can be tested statistically using

630 ANOVA on summary statistics describing the curves.

631

632 **Figure 6.** A) Butyrate concentration time profile, normalized by the simulated *F.*

633 *prausnitzii* biomass, for coculture and monoculture. B) Simulated species composition.

634

635 **Supplemental figure legends:**

636 **Figure S1.** Simulated glucose concentration.

637 **Figure S2.** Biomass normalized acetate concentration.

638 **Figure S3.** Simulated fluxes of key reactions in the butyrate fermentation pathway in *F.*

639 *prausnitzii*, for high glucose concentration, at time zero and 5 hours.

640 **Figure S4.** Simulated butyrate secretion fluxes in *F. prausnitzii*, under secondary

641 maximization/minimization of butyrate or lactate production, as a function of phosphate

642 concentration, in low glucose conditions.

643

644

645

646

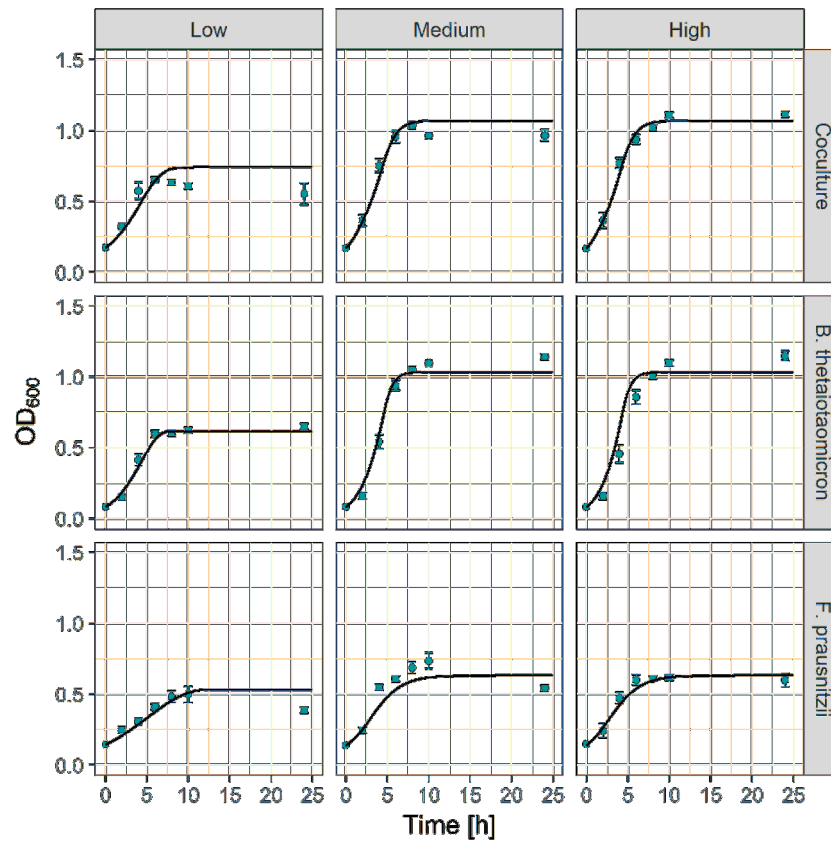


Figure 1. Optical densities for single species and coculture of *F. prausnitzii* and *B. thetaiotaomicron*, grown in three different media conditions. The simulations (solid curves) were obtained by dFBA with the same set of uptake parameters for all media conditions. The columns correspond to the media conditions while the rows correspond to the cultured species.

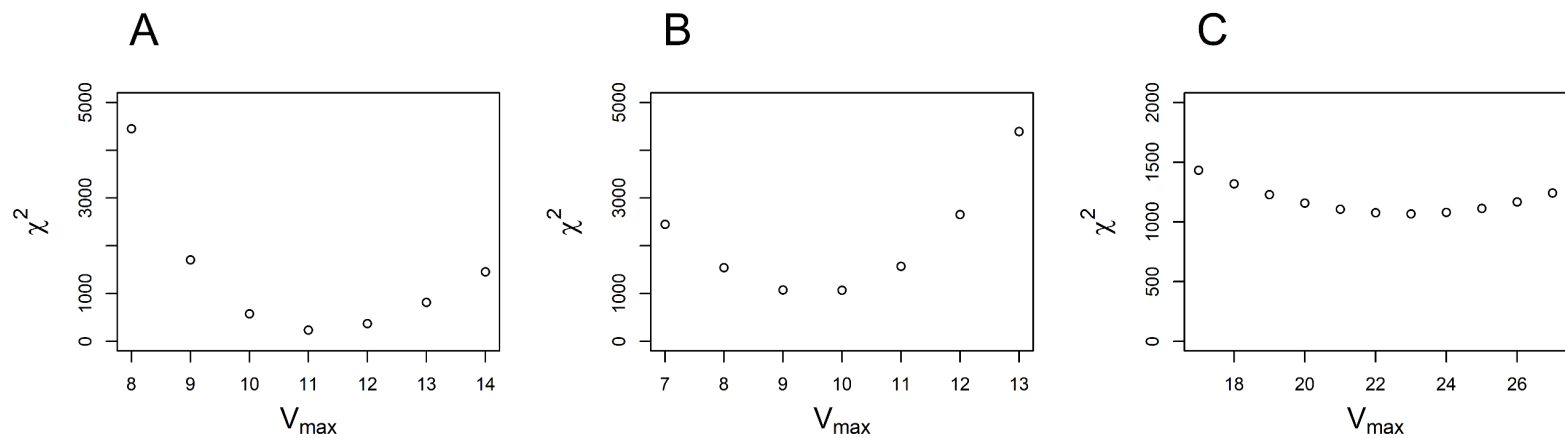


Figure 2. The sensitivity of the OD curves to the values of the maximum nutrient uptake parameter V_{max} . The values of the V_{max} parameter used in the simulations were obtained by minimizing c^2 , the sum of the squared deviations of the simulation from the experimental values, weighted by the measured variance. We used a single value of V_{max} for the uptake of all nutrients by the *B. thetaiotaomicronn* model, with the minimum of minimizing c^2 , shown in panel A). In the case of *F. prausnitzii*, we determined two separate values of minimizing c^2 , one for glucose and acetate uptake shown on panel B), and another one for the rest of the nutrients, shown on panel C).

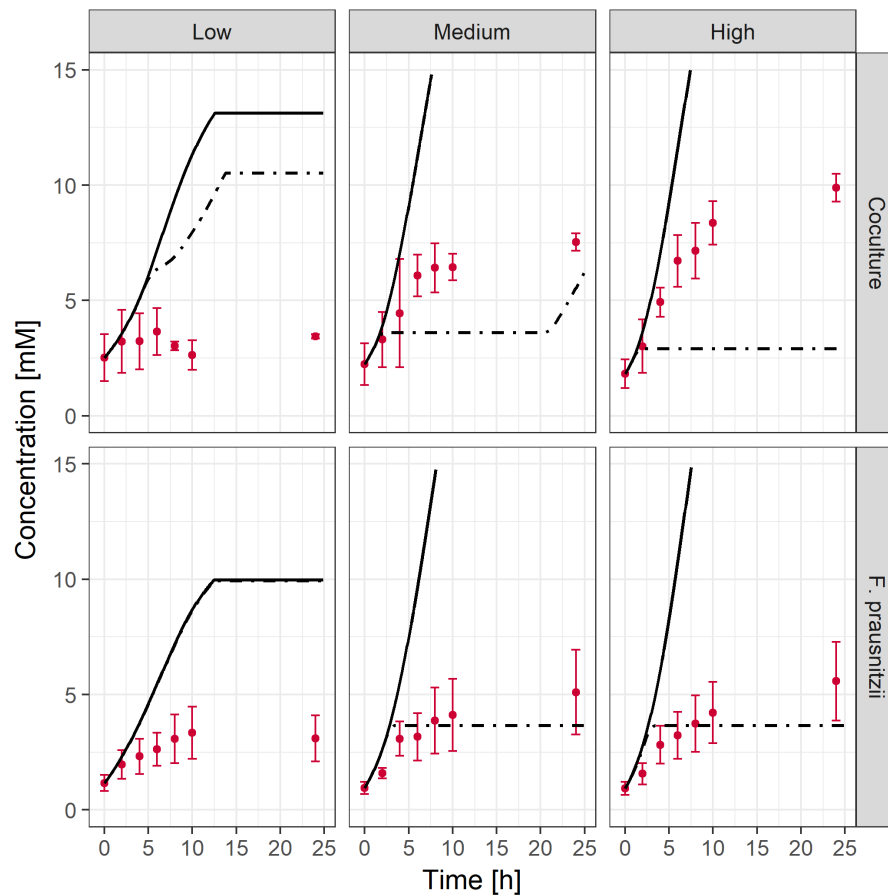


Figure 3. Experimental and simulated (solid, dot and dash curves) butyrate production time courses for monocultures and coculture under the three initial glucose/acetate initial concentrations. Apparent differences demonstrated in these plots in butyrate production for *F. prausnitzii* monoculture vs. coculture and for the three initial concentrations can be tested statistically using ANOVA on summary statistics describing the curves. The simulated curves correspond to the maximized (solid curve) and minimized (dash dot curve) butyrate secretion.

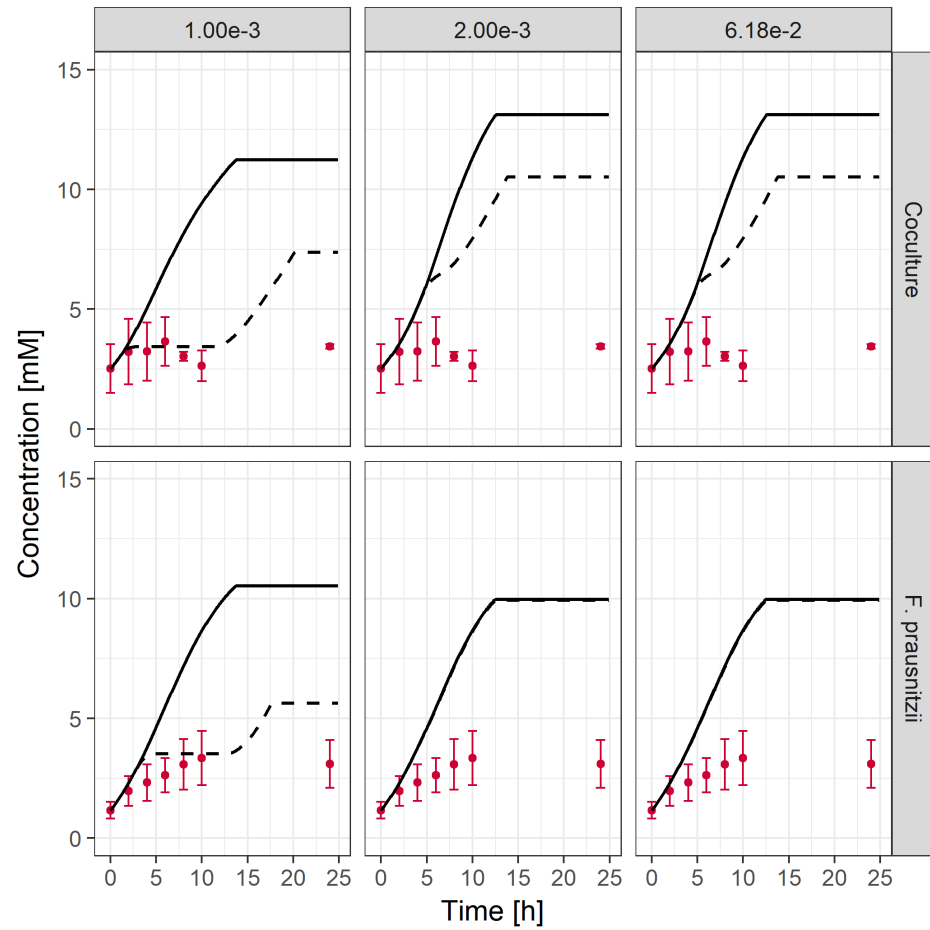


Figure 4. Simulated butyrate production for three starting abundances of phosphate for the low initial acetate/glucose concentration. Lowering of the phosphate concentration leads to multiple FBA solutions and difference between secondary minimization and maximization of butyrate secretion.

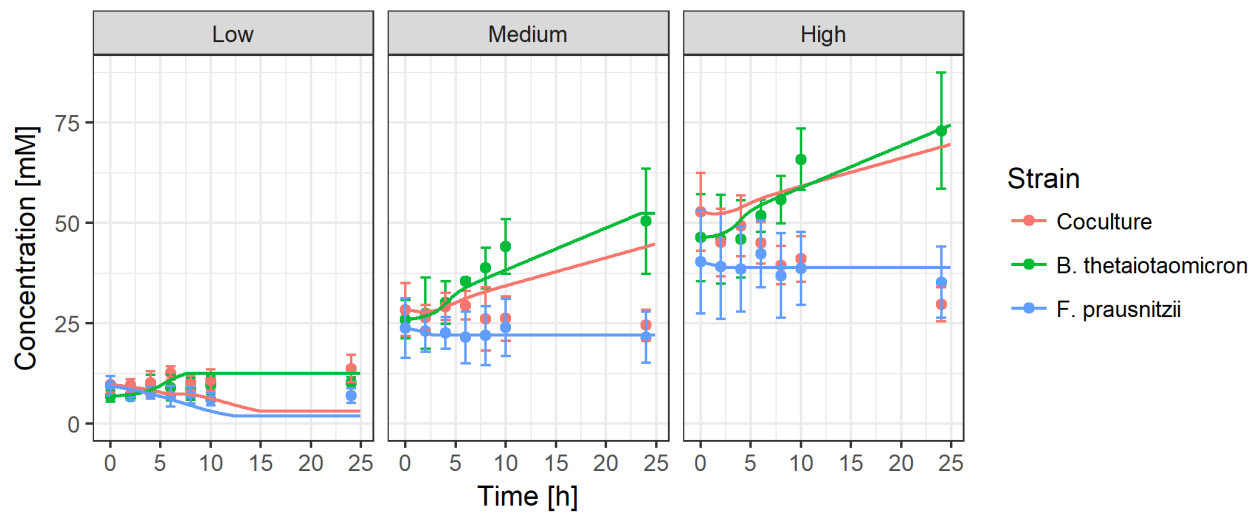
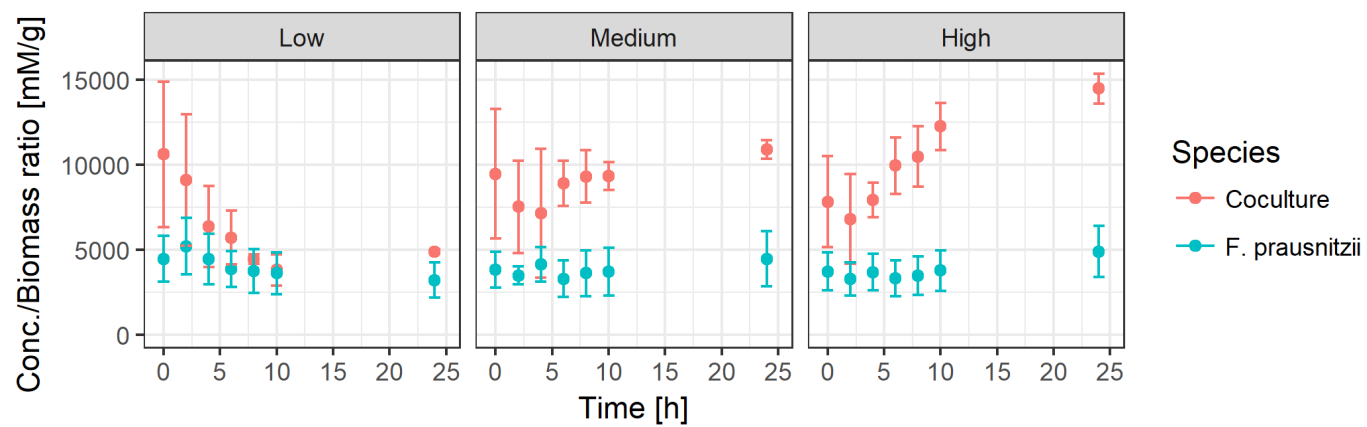


Figure 5. Experimental and simulated (solid curves) acetate production time courses for monocultures and coculture under the three initial glucose/acetate initial concentrations. Apparent differences demonstrated in these plots in butyrate production for *F. prausnitzii* monoculture vs. coculture and for the three initial concentrations can be tested statistically using ANOVA on summary statistics describing the curves.

A



B

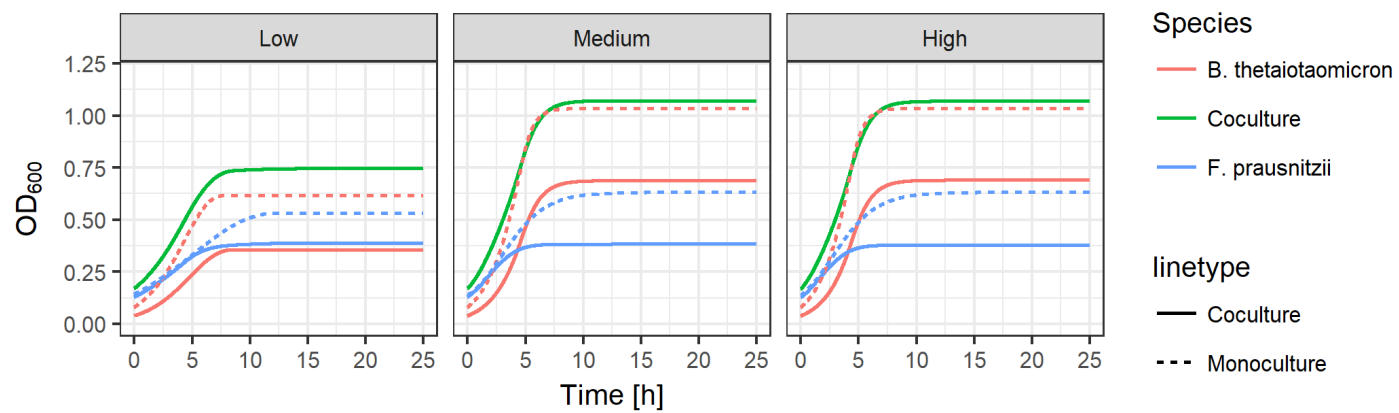


Figure 6. A) Butyrate concentration time profile, normalized by the simulated *F. prausnitzii* biomass, for coculture and monoculture. B) Simulated species composition.